Research article

Intervaginal space injection of photothermal chemotherapy nanoparticles for facilitating tumor targeting and improving outcomes in mice

Yuling Liu [1], Meng Su [1], Yinghan Wang, Yilong Du, Yan Wang, Nan Hu [*]

Key Laboratory of Traditional Chinese Medicine Research and Development, Chengde Medical University, Chengde, 067000, China

ARTICLE INFO

ABSTRACT

Although numerous photothermal nanoparticles have been designed to improve the enhanced and permeability and retention (EPR) effect, the delivery of nanoparticles to the tumor site remains a major obstacle in cancer treatment. The interstitial structure and its internal fluid that play an important role in material transmission, intercellular signal transduction, tissue morphology, immunity, tumor development, and disease diagnosis and treatment may be considered as a new route for drug delivery. Here, we prepared a nanoplatform composed of polydopamine (PDA), indocyanine green (ICG) as a photothermal agent, and paclitaxel (PTX) as a chemotherapeutic drug. The designed PDA-ICG nanoparticles displayed excellent photothermal conversion ability, with the synergistic effect of PTX, the growth of MDA-MB-231 cells was significantly suppressed with the cell viability of 6.19% *in vitro*. Taking advantage of bioimaging ability of ICG, tumor-targeting of the nanoparticles injected into the interstitial space was study, Compared with intravenous injection, nanoparticles better targeted the tumor based on the interstitial fluid flow in MBA-MD-231 bearing mice. Furthermore, the antitumor efficacy was studied *in vivo*. With the improved accumulation of PDA-ICG-PTX nanoparticles injected into the interstitial space and the synergistic effect of photothermal therapy and chemotherapy, tumor growth was inhibited without obvious side effects. These results demonstrated that interstitial space injection may be a superior administration route for tumor-targeting nanoparticles. The PDA-ICG-PTX nanoparticles delivered via the interstitial space exhibit great potential in the photothermal chemotherapy of cancers.

1. Introduction

In antitumor treatment, hyperthermia has become an attractive effective physical therapy and is mainly used as an adjuvant for chemotherapy and radiotherapy [1,2]. When the temperature inside the tumor exceeds 41.5 °C, cytotoxicity occurs, and a temperature above 43 °C severely damages tumor cells [3]. Combined with chemotherapy, the antitumor effect is greatly enhanced, while unwanted chemotherapy effects will be reduced. With the development of nanotechnology, nanomaterials are increasingly and successfully used in biological application and antitumor treatments [4–7]. The properties of nanomaterials such as easy modification,

large surface-to-volume ratio, and controllable size and shape enable them to increase the solubility of drugs, improve their stability, and enhance their bioavailability. In addition, the strong absorption of infrared light and the photothermal conversion efficiency of nanomaterials make them ideal agents for the photothermal therapy of tumors. Locally accumulated nanomaterials can convert luminous energy into heat, resulting in an increased temperature in the tumor tissue. Thus, tumor cells are killed, whereas healthy surrounding tissue is not impacted. Therefore, nanomaterial-mediated photothermal therapy is considered "green therapy" and is increasingly combined with chemotherapy.

Nanomaterial delivery is a crucial factor in antitumor treatment. The commonly used administration route is intravenous injection (IVI). Injected nanomaterials reach the tumor vessels with the systemic blood circulation and then leak into the tumor interstitium through diffusion and convection. Subsequently, nanomaterials in the tumor interstitium are transported to the target cells. The tumor microenvironment including structural and functional abnormalities of tumor vessels and the elevated interstitial fluid pressure substantially impede nanomaterial transport [8,9]. How to enhance permeability and improve retention of nanomaterials in tumors after systemic administration remains a difficult hot topic [10]. Although satisfactory results have been reported, the tumor microenvironment is still an obstacle to drug delivery. According to preclinical data, only 0.7% of IVI-administered nanomaterials accumulate in tumor tissues, and EPR effect are disputed [11–13]. This largely limits the biological application of nanomaterials in cancer treatment, and the development of novel administration routes to improve the delivery of nanoparticles (NPs) is vital.

So far, interstitial structures have been largely ignored, and only half a century ago, the physiological and pathological significance of interstitial structures has been recognized. Recent studies suggest that interstitial structures distributed throughout the entire body should be regarded as an organ. The interstitial spaces are composed of a continuous fibrous network that may be connected within tissues and organs, as well as between different tissues and organs. The interstitium with its interstitial fluid has been likened to a "highway" that may facilitate the spreading of tumor cells under pathological conditions [14–16]. Moreover, long-distance transportation via interstitial fluid occurs throughout the interstitial space of the body along with that via the blood vessels. It should be considered a novel systemic circulation distinct from blood circulation and can be a novel route for organ-targeted extravascular drug delivery [17–19].

In this study, we prepared NPs for photothermal chemotherapy composed of three agents: (1) polydopamine (PDA) with its adjustable diameter, biocompatibility, biodegradability, and photothermal conversion properties is commonly utilized as a photothermal agent in photothermal therapy; (2) indocyanine green (ICG) is also a popular photothermal agent to increase photothermal efficacy and is used for near-infrared (NIR) bioimaging; and (3) paclitaxel (PTX) is a chemotherapeutic drug widely used in the treatment of solid tumors. These PDA-ICG-PTX NPs were administered via IVI or intervaginal space injection (ISI). By comparing intratumoral NP accumulation, we confirmed ISI as an NPs delivery route that can target tumors with minimal systemic toxicity. Our work presents a reliable strategy to improve cancer treatment based on the synergistic effect of photothermal therapy and chemotherapy of PDA-ICG-PTX NPs injected via ISI and expends the delivery route of NPs.

2. Method details

2.1. Materials

Dopamine hydrochloride was purchased from J&K Scientific Co., Ltd. (Beijing China). Ammonium hydroxide and anhydrous ethanol were purchased from Beijing Chemical Reagent Company (Beijing, China). ICG and PTX were purchased from Sigma-Aldrich (St. Louis, USA). DAPI Staining Solution was provided by Invitrogen (USA). Phosphate-buffered saline (PBS), 4% paraformaldehyde, Roswell Park Memorial Institute (RPMI-1640), and penicillin-streptomycin were purchased from Solebao Biotechnology Co., Ltd. (Beijing, China). Fetal bovine serum was purchased from Zhejiang Tianhang Biotechnology Co., Ltd (Hangzhou, China). Cell Counting Kit-8 (CCK-8) was purchased from Dojindo Molecular Technologies (Kumamoto Techno, Japan). The MDA-MB-231 cell line was obtained from the American Type Culture Collection (ATCC, Manassas, USA).

2.2. Synthesis of PDA–ICG NPs

A total of 1.5 mL ammonium hydroxide (28–30%) was added to a mixture of 40 mL anhydrous ethanol and 90 mL deionized water, then placed in a water bath with a temperature of 37 °C, and magnetic stirring (300 r/min) was performed for 30 h. Subsequently, 0.5 g of dopamine hydrochloride dissolved in 10 mL of deionized water was added to the aforementioned solution. After 30 h, the solution was centrifuged at 11,000 r/min for 15 min, followed by washing with deionized water three times, and PDA NPs were obtained after lyophilization. Next, 4 mg of ICG were mixed with 4 mL PDA NPs (1.9 mg/mL) and suspended in a mixture of water and DMSO (10:1, v/v). This solution was incubated at room temperature for 12 h with magnetic stirring (300 r/min), followed by centrifugation at 11,000 r/min and 38,000 r/min for 10 and 60 min, respectively. Finally, the supernatant was removed, and the sediment was washed with deionized water three times to obtain PDA-ICG NPs.

2.3. Synthesis of PDA-ICG-PTX NPs

In total, 10 mg of PDA-ICG NPs and 3 mg of PTX were dispersed in 3 mL acetone at room temperature. After 2/3 of the acetone volume had evaporated, PTX-coated PDA-ICG NPs were collected by centrifugation and washed three times with deionized water to remove PTX adsorbed on the surface and obtain PDA-ICG-PTX NPs.

2.4. Morphology

NP-containing solutions were dripped on 40-mesh copper grids. After evaporation, the samples were scanned using a transmission electron microscope (TEM; Ht-7700, Hitachi, Japan), and the fluorescence spectra were recorded using a fluorescence and absorbance spectrophotometer (HITACHI 7100, Hitachi).

2.5. Photothermal effect and stability

Solutions containing free ICG, PDA-ICG, or PDA-ICG-PTX were irradiated with an 808 nm laser at a power density of 1.4 W/cm^2 for 10 min. The temperature was monitored using an infrared thermal imaging camera (FLIR S60, USA). To further investigate the stability of PDA-ICG-PTX NPs after irradiation, NPs dispersion (500 µg/mL) was irradiated with 808 nm laser (1.4 W/cm^2) for 4 min and then turn off the laser, temperature was recorded every 20 s until cooled to room temperature, the operation cycle was repeated four times. Additionally, photothermal conversion efficiency (η) was calculated as per the references reported [20].

2.6. Drug release rate

PDA-ICG-PTX solutions (500 µg/mL) were irradiated with 808 nm laser (1.4 W/cm^2) for 5 min and then added to the dialysis bags (MWCO: 3500Da), the bags were placed in the shakers containing PBS (pH 6.5 or pH 7.4) with a stirring speed of 120 rpm at 37 °C. At the designed time point, 1 mL medium was taken out and the same volume PBS was added, the concentration of PTX released was measured by HPLC [21].

2.7. Cellular uptake

MDA-MB-231 cells were seeded into a 20 mm glass bottom cell culture dish, cultured in RPMI-1640 containing 10% fetal bovine serum and 1% penicillin-streptomycin for 12 h, and then incubated with PDA-ICG-PTX NPs in the dark at 37 °C for another 12 h. After removal of the medium, cells were washed with PBS three times and fixed with 4% paraformaldehyde for 20 min at room temperature. Residual paraformaldehyde was washed out using PBS, 1 mL 4',6-diamidino-2-phenylindole (DAPI) was added, and the cells were incubated in the dark at room temperature for 7 min. The dyed cells were kept in PBS and imaged using a confocal fluorescence microscope (Olympus FV 1000) with an excitation wavelength of 640 nm.

2.8. Photothermal chemotherapy effect in vitro

MAD-MB-231 cells at a density of 3×10^4/mL were seeded into 96-well plates and cultured for 6 h in the dark at 37 °C. Then PDA-ICG or PDA-ICG-PTX NPs were added to the medium. After co-incubation for 12 h, the cells were irradiated with an 808 nm laser at a power density of 1.4 W/cm^2 for 1, 2, or 5 min. After irradiation, the cells were cultured for another 24 h. Cytotoxicity was tested using the CCK-8 assay.
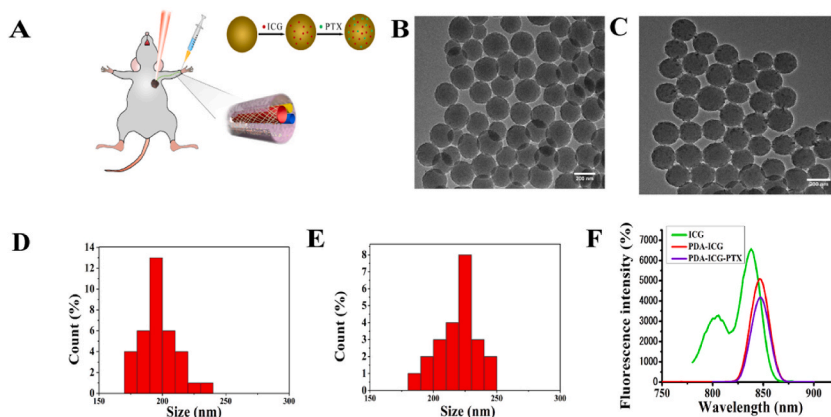
Fig. 1. Characterization of the nanoparticles. (A) Schematic illustration of the PDA-ICG-PTX NP preparation and their administration via inter-vaginal space injection. (B) TEM image of PDA NPs and (C) PDA-ICG-PTX NPs. Scale bar = 500 nm. (D) Particle size of PDA NPs and (E) PDA-ICG-PTX NPs. (F) Fluorescence spectra of free ICG, PDA-ICG NPs, and PDA-ICG-PTX NPs. ICG, indocyanine green; NP, nanoparticle; PDA, polydopamine; PTX, paclitaxel; TEM, transmission electron microscopy. (For interpretation of the references to colour in this figure legend, the reader is referred to the Web version of this article.)

2.9. Tumor xenografts and tumor-target imaging

The animal experiments were reviewed and approved by the Animal Ethics Committee of Chengde Medical University. Female BALB/c nude mice (4–6 weeks) were purchased from Beijing Huafukang Biotechnology Co., Ltd (Beijing, China). A total of 2×10^6 MDA-MB-231 cells were injected into the mammary pads of these mice to establish an orthotopic breast tumor xenograft model. When tumor diameters reached 3–4 mm, NPs were injected into the interstitial space of the carpal canal as per Fig. 1A indicated in the ISI group or into the tail vein in the IVI group. Before and after injection, the *in vivo* spectrum imaging system IVIS Lumina III (Perki-nElmer, USA) was used to record real-time NIR fluorescent images at the respective time points. Mice were sacrificed 24 h after the injection. and the tumors, hearts, livers, spleens, lungs, and kidneys were removed to analyze fluorescence intensity *ex vivo*. Tumor-bearing nude mice received PDA-ICG-PTX NPs via ISI, and photoacoustic signals (PAs) were obtained by fast multispectral opto-acoustic tomography (MSOT; inVision 128, iThera medical, Germany).

2.10. In vivo photothermal chemotherapy

Tumor-bearing mice were divided into PDA-ICG-PTX + IVI, PDA-ICG + ISI, and PDA-ICG-PTX + ISI groups (n = 5 each). After NPs administration, laser treatment was carried out twice at a power density of 1.7 W/cm² for 5 min each with a 1 min interval. Infrared thermal images of the tumor were obtained. Treatment was performed once a week, and tumor sizes were measured every 2 days. The tumor volume was calculated using the following formula: volume = (tumor length) × (tumor width)²/2. On day 21, mice were sacrificed, and tumors were dissected and weighed. Tissue samples from the tumor and visceral organs (heart, liver, spleen, lung, and kidney) were stained with hematoxylin and eosin (H&E) for histological analysis.

2.11. Statistical analysis

All experimental data were expressed as means ± standard deviation using SPSS 26.0 sofeware. One-way analysis of variane (ANOVA) or two-way ANOVA was used to compare differences among groups after normal distribution test, and followed by the Bonferroni or Games-Howell test for multiple comparisons. Graphs were plotted with OriginPro 8.5 software. $p < 0.05$ was considered statistically significant.

3. Results

3.1. Characterization of the nanoparticles

PDA, a kind of artificial melanin material that is obtained from dopamine self-polymerization under alkaline conditions, is widely used in photothermal therapy [22–26]. The NIR fluorescent dye ICG is approved by the United States (US) Food and Drug Admin-istration (FDA) for clinical bioimaging use such as in laparoscopic cholecystectomy [27,28] and angiography [29,30]. Moreover, ICG is utilized as a photosensitizer in photothermal therapy [31,32]. As a traditional chemotherapeutic agent, PTX is often used in the treatment of breast cancer [33], ovarian cancer [34], and lung cancer [35]. In the present study, PDA-ICG-PTX NPs were synthesized for the expected synergistic effects of photothermal therapy and chemotherapy. TEM (Fig. 1B) showed that PDA NPs were regular spheres with smooth surface and an average diameter was 196.05 ± 13.67 nm (Fig. 1D), when ICG was conjugated, the diameter
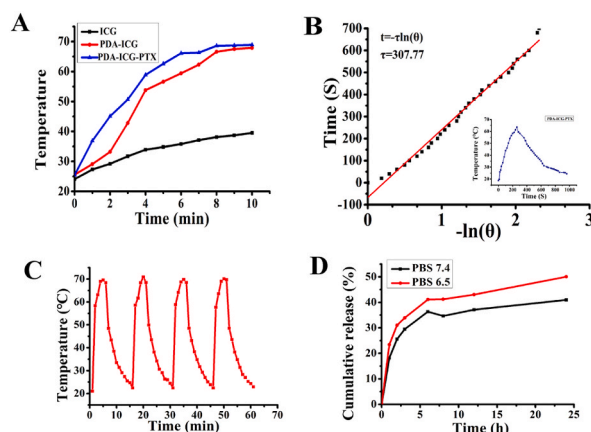
Fig. 2. Photothermal performance and drug release of PDA-ICG-PTX NPs. (A) Heating curves of free ICG, PDA-ICG NPs, and PDA-ICG-PTX NPs after laser irradiation. (B) Linear fitting of time data versus -ln(θ) from the cooling period of PDA-ICG-PTX NPs (808 nm, 1.4 W/cm²). (C) Temperature change of PDA-ICG-PTX NPs during 4 cold and hot cycles. (D) Cumulative release curves of PTX at different pH (6.5, 7.4) after irradiation (808 nm, 1.4 W/cm²).

changed to 200.66 ± 6.94 nm, after PTX loaded, the surface was rough with spiny granules on it (Fig. 1B) and the average diameter increased to of 224.36 ± 23.86 nm (Fig. 1E), both of which confirmed PTX was loaded. The fluorescence spectra of ICG, PDA-ICG, and PDA-ICG-PTX NPs in aqueous dispersion were obtained by fluorospectrophotometry. The spectrum of free ICG displayed a maximum peak at 838 nm, whereas the peaks of PDA-ICG and PDA-ICG-PTX were slightly shifted to 846 nm due to the interaction of the π-π conjugate between PDA and ICG (Fig. 1F) [36]. These results also indicated that ICG was successfully loaded onto PDA NPs.

3.2. Photothermal performance and drug release rate

Photothermal agents must have outstanding properties regarding NIR absorption and photothermal effect. The photothermal conversion by free ICG, PDA-ICG, and PDA-ICG-PTX was monitored by Infrared thermal imaging, using the same concentration (50 μg/mL) under 808 nm laser irradiation (1.4 W/cm^2) over 10 min. As shown in Fig. 2A, the temperatures of PDA-ICG and PDA-ICG-PTX NPs increased rapidly to almost 70 °C, whereas the temperature of free ICG remained below 40 °C. The enhanced photothermal ability results from the synergistic effect of PDA and ICG. To further estimate the photothermal performance of PDA-ICG-PTX NPs (Fig. 2B), the photothermal conversion effficiency (η) was calculated and the value was 22.28%.

Then the photostability of PDA-ICG-PTX NPs was evaluated, during 4 cold thermal cycle, there was no significant changes of the temperature obtained, which showed excellent photostability (Fig. 2C). Moreover, PTX release rates after irradiation in pH 6.5 and pH 7.4 were investigated, respectively. The cumulative release reached to 50.05% by 24 h in PBS of pH 6.5, which was higher than that of pH 7.4 (Fig. 2D), this results may due to the weak acidic condition facilitated the release of PTX.

It has been reported that a locally higher temperature (40–43 °C) in the tumor may destroy malignant cells [37]. Our results indicated that PDA-ICG-PTX NPs can be used as an excellent photothermal agent for photothermal therapy in further *in vitro* and *in vivo* experiments.

3.3. Cellular uptake

To explore the cellular uptake of the NPs, MDA-MB-231 cells were incubated with PDA-ICG-PTX NPs for 12 h. Laser scanning confocal microscopy was used to assess the internalization of NPs. The blue fluorescence was the DAPI signal after laser light excitation at 405 nm, and the red fluorescence indicated PDA-ICG-PTX NPs after laser light excitation with a wavelength of 640 nm (Fig. 3A). The results illustrated that PDA-ICG-PTX NPs were effectively taken up into the cytoplasm.

3.4. Photothermal chemotherapy effect in vitro

Next, we investigated the antitumor effect of the NPs *in vitro*. When PDA-ICG NPs were incubated with MDA-MB-231 cells for 24 h, cell cytotoxicity was not observed for concentrations up to 100 μg/mL, demonstrating the biosafety of PDA-ICG NPs. However, when PDA-ICG-PTX NPs were added to the cells, dose-dependent cytotoxicity occurred due to chemotherapeutic PTX effects. As shown in Fig. 3B, cell viability decreased from 72.5% at 20 μg/mL PDA-ICG-PTX NPs to 53.3% at 100 μg/mL. Then, we evaluated the synergistic effect of photothermal therapy and chemotherapy for the PDA-ICG-PTX NPs at concentration of 50 μg/mL. After incubation with NPs for 12 h, cells were irradiated with 808 nm laser light (1.4 W/cm^2) for 1, 2, or 5 min. Compared to the same time point, cell viability in the PDA-ICG-PTX group was lower than that in the PDA-ICG group, when irradiated for 5 min, cell viability was 6.19%, which was 3.57 times decreased than that in PDA-ICG group (Fig. 3C). This enhanced cytotoxicity demonstrated the synergistic effect of photothermal
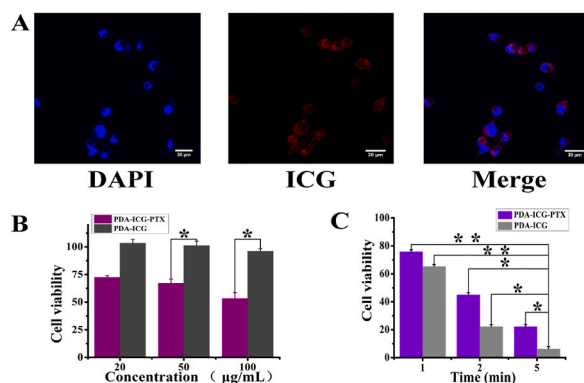
Fig. 3. Cellular uptake and anti-tumor effects *in vitro*. (A) Laser scanning confocal microscopy of MDA-MB-231 cells incubated with PDA-ICG-PTX NPs (Blue: DAPI, red: ICG). Scale bar = 30 μm. (B) Cell viability of MDA-MB-231 cells incubated with different concentrations of PDA-ICG NPs or PDA-ICG-PTX NPs. (C) Cell viability of MDA-MB-231 cells incubated with PDA-ICG NPs or PDA-ICG-PTX NPs followed by 808 nm laser irradiation at an intensity of 1.4 W/cm^2 for the specified time. Data were presented as means ± s.d. (n = 3 per group; two-way ANOVA followed by Bonferroni test for multiple comparisons). *$p < 0.05$, **$p < 0.01$. ICG, indocyanine green; NP, nanoparticle; PDA, polydopamine; PTX, paclitaxel. (For interpretation of the references to colour in this figure legend, the reader is referred to the Web version of this article.)

therapy and chemotherapy. Moreover, cell viability in the PDA-ICG-PTX group was time-dependent. These findings suggested that PDA-ICG-PTX NPs with laser irradiation exert a synergistic antitumor effect *in vitro*.

3.5. Tumor targeting after ISI

To assess the tumor-targeting efficacy of PDA-ICG-PTX NPs administered by ISI (the injection point was displayed in Fig. 1A, briefly, nanoparticles were injected into the interstitial space of the wrist canal that wraped around nerves and blood vessels. In the interstitial space, the nanoparticles was transported to the tumor with the interstitial fluid flow [38]). orthotopic MDA-MB-231 tumor-bearing mice were divided into two groups, i.e., the ISI group and the IVI group. After the injection of 0.1 mL PDA-CG-PTX NPs (500 µg/mL), the ICG fluorescence signal was obtained by NIR fluorescence imaging. In the ISI group (Fig. 4A), the fluorescence signal was detected only at the injection site of the forearm 1 h after administration, then the signal was obtained at the tumor site over time. At 24 h, the signal extended to the left chest of the mice. Tumor and vital organs were excised after 24 h. A prominent signal was observed in the tumor, whereas the liver showed a weak signal. By contrast, the fluorescence signal in the IVI group was detected in the abdominal region. After 24 h, signals were found *in vitro* in the lung and liver but not in the tumor (Fig. 4B).

To further confirm the PDA-ICG-PTX NPs accumulation in tumor tissue, deep-tissue high-resolution MSOT was used to validate the tumor-targeting efficacy after ISI. Fig. 4C demonstrated definite MSOT signals inside the tumor, and with progressing time, the signal proportion increased. Thus, the optoacoustic signals of PDA-ICG-PTX NPs evidenced the superior tumor-targeting ability of ISI.

3.6. In vivo photothermal effect of PDA-ICG-PTX NPs after ISI

To investigate the differences in photothermal effects between ISI and IVI, orthotopic MDA-MB-231 breast tumor-bearing nude mice were divided into three groups: a control group without treatment, an IVI group, and an ISI group. In the ISI and IVI groups, animals were 3 h after NPs injection exposed to 808 nm laser treatment ($1.7 \ W/cm^2$) for 5 min. Infrared thermal imaging was used to monitor the temperature (Fig. 5A) reaching 36.4 °C in the control group, 40.0 °C in the IVI group, and 45.7 °C in the ISI group. The temperature difference between the IVI and ISI groups may be due to the superior accumulation of PDA-ICG-PTX NPs after ISI, which was consistent with the NIR fluorescence and PA imaging results.

In this study, the laser intensity was set to $1.7 \ W/cm^2$, and the intratumoral temperature reached up to 45.7 °C, which did not fully inhibit tumor growth. However, when the laser intensity was set to $2.0 \ W/cm^2$, the intratumoral temperature reached up to 50 °C, the tumors disappeared, but skin lesions occurred (Supplementary Fig. 1). Thus, a temperature below 45 °C is suitable without damaging the surrounding healthy tissue [39].

3.7. In vivo photothermal chemotherapy effect and safety evaluation

Based on the excellent accumulation of NPs at the tumor site after ISI, the chemophotothermal effect of PDA-ICG-PTX NPs was
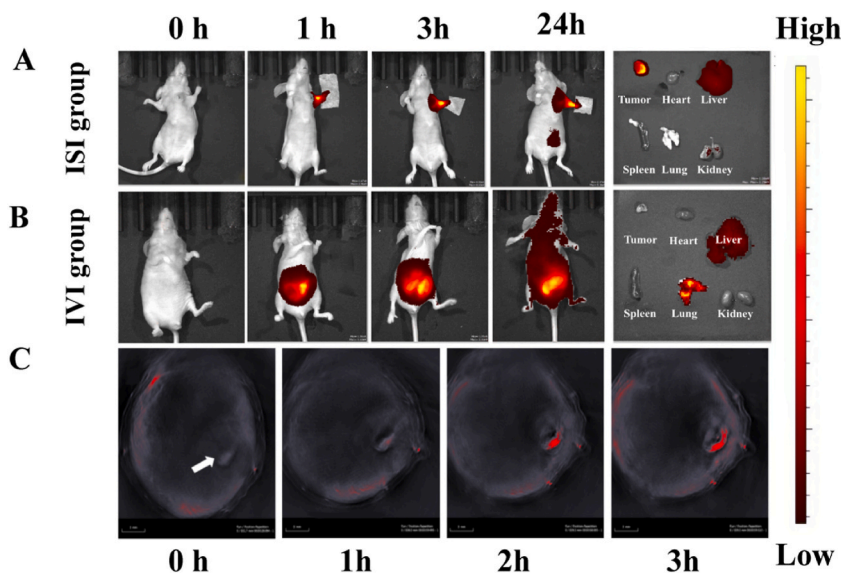

Fig. 4. Detection of PDA-ICG-PTX NPs following their intervaginal space injection (ISI) into tumor-bearing mice. (A, B) Real-time NIR fluorescence images of tumor-bearing mice *in vivo* and tumor tissue and organs *ex vivo* after ISI (A) and IVI (B) of PDA-ICG-PTX NPs. (C) MSOT of PDA-ICG-PTX NPs on transections of tumor regions at different time points. The white arrow indicates the tumor. ICG, indocyanine green; ISI, intervaginal space injection; IVI, intravenous injection; MSOT, multispectral optoacoustic tomography; NIR, near-infrared; NP, nanoparticle; PDA, polydopamine; PTX, paclitaxel. (For interpretation of the references to colour in this figure legend, the reader is referred to the Web version of this article.)
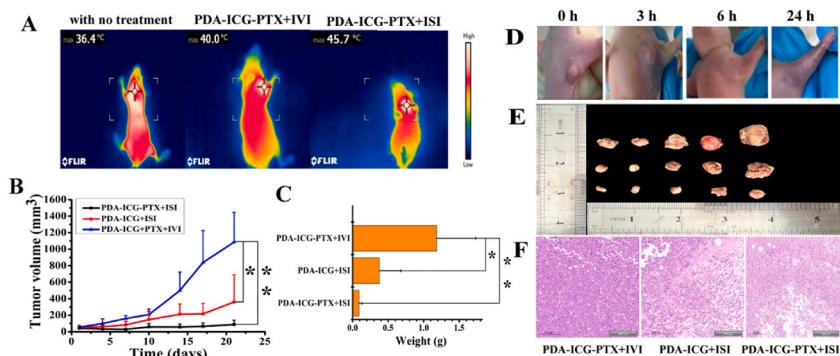
Fig. 5. Antitumor effects of photothermal chemotherapy *in vivo*. (A) Infrared thermal images of tumor-bearing mice after 808 nm laser irradiation (1.7 W/cm², 5 min) in different groups. (B) Tumor growth over 21 days after the first treatment. (C) Tumor weight in the study groups on day 21. (D) Tumor morphology at different time points after the first ISI treatment with PDA-ICG-PTX NPs *in vivo*. (E) Images of excised tumors on day 21. **(F)** H&E-stained tumor sections after the respective treatment. (Scale bars = 20 μm). Data were presented as means ± s.d. (n = 5 per group; one-way ANOVA followed by Games-Howell for multiple comparisons).*p < 0.05, **p < 0.01. H&E, hematoxylin and eosin; ICG, indocyanine green; ISI, intervaginal space injection; NP, nanoparticle; PDA, polydopamine; PTX, paclitaxel. (For interpretation of the references to colour in this figure legend, the reader is referred to the Web version of this article.)

investigated. Animals were divided into three groups: PDA-ICG-PTX + IVI, PDA-ICG + ISI, and PDA-ICG-PTX + ISI. The tumor sites were laser-irradiated 3 h after NPs injection. As shown in Fig. 5B, the tumor volume in the PDA-ICG-PTX + IVI group grew rapidly possibly due to insufficient number of photothermal agents at the tumor site. Although enough NPs accumulated at the tumor site after ISI, tumor growth in the PDA-ICG + ISI group was only controlled to a certain extent. In the PDA-ICG-PTX + ISI group, tumor growth was strongly suppressed. Furthermore, tumors in the PDA-ICG-PTX + ISI group were ablated after the first treatment (Fig. 5D). On day 21, animals were sacrificed by intraperitoneal injection of an anesthetic overdose, and the tumors were excised and weighed. The average tumor weight of the PDA-ICG + ISI group was significantly lower than those of the PDA-ICG-PTX + IVI and PDA-ICG + ISI groups, decreased by 13 times and 4 times, respectively (Fig. 5C and E). In H&E-stained tumor sections, more necrosis was observed in the PDA-ICG-PTX + ISI group than that in the other two groups (Fig. 5F). These results indicated that photothermal therapy alone was not sufficient to prevent tumor growth, whereas photothermal therapy with chemotherapy displayed excellent synergistic antitumor effects.

Finally, the biosafety of PDA-ICG and PDA-ICG-PTX NPs was investigated after IVI and ISI. Major organs were histologically analyzed. In the PDA-ICG-PTX + IVI group, hepatic edema (Fig. 6) was observed in addition to skin lesions (Supplementary Fig. 2). The potential accumulation of NPs in the liver may cause these unwanted chemotherapy effects. No structural damage was found in the PDA-ICG + ISI and PDA-ICG-PTX + ISI groups. These results suggested that NPs administered by ISI may decrease the systemic toxicity of chemotherapeutic drugs. ISI-administered PDA-ICG-PTX NPs may serve as a safe and efficient nanoplatform for photothermal chemotherapy.
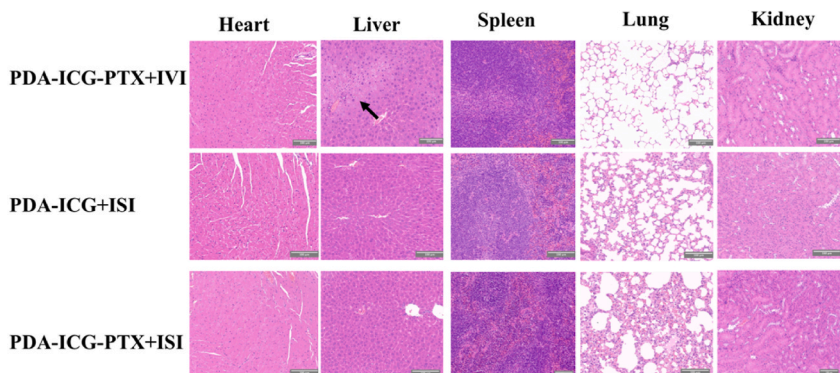
Fig. 6. Biosafety of nanoparticles after IVI and ISI. H&E staining of vital organs in the different study groups. The black arrow points to edema of the liver in the PDA-ICG-PTX + IVI group (Scale bars = 100 μm). H&E, hematoxylin and eosin; ICG, indocyanine green; ISI, intervaginal space injection; IVI, intravenous injection; PDA, polydopamine; PTX, paclitaxel. (For interpretation of the references to colour in this figure legend, the reader is referred to the Web version of this article.)

4. Discussion

One of the primary challenge in the photothermal chemotherapy of cancer treatment is to increase the delivery of NPs to the tumor site. Most of the recent researches have focus on the improvement of EPR effect, but NPs delivery remains insufficient in a meta-analysis of cancer-targeting nanomedicine [40]. The most common administration route for NPs is IVI. Compared with normal blood vessels, blood vessels in tumors are irregularly twisted, with high blood flow resistance, low flow velocity, and uneven distribution. Additionally, the blood vessel density in the tumor core is much lower than that in its periphery, and the ratio of avascular areas to blood-filled areas is higher. These changes lead to insufficient blood supply to tumor tissue, which affects NPs delivery. Moreover, due to extracellular matrix proliferation in the tumor stroma, the interstitial pressure increases substantially which further reduces NPs translocation from blood vessels to the tumor tissue [41,42]. In addition, the size of NPs is a key factor in their delivery after IVI; particle sizes below 20 nm can efficiently penetrate the extracellular matrix from the blood vessels, whereas particles with sizes of 100 and 200 nm barely extravasate (<5%) [9,43]. Our results are consistent with these reports. In the IVI group, PDA-ICG-PTX NPs with a size of 200 nm are not detected in tumor tissue.

On account of the limitations of IVI, we exert another type of administration way named intervaginal space injection (ISI). Prior studies have demonstrated that ISI is a new type of drug administration that is based on the interstitium distributed over the entire body. Within its hierarchical multiphase porous medium (a micrometer-scale hydrophobic fiber network filled with a nanometer-scale hydrophilic porous medium), interstitial fluid transported inside takes action on the delivery of matter and messages [44–46]. In our previous research, liquid metal is injected into the interstitial space of the carpal canal in $B_{16}F_{10}$-bearing mice, the metal is transported inside the perivascular interstitial space, which is always accompanied by nerves and blood vessels, from the fingertip to the axillary region and TEM results indicate that the injected liquid metal circulates through the tumor-penetrating fiber network in the stroma and transports into the tumor [38].

According to these investigations, we deduce that PDA-ICG-PTX NPs injected by ISI transport in the interstitial space to the tumor site, then tumor interstitium may facilitate the delivery of NPs: the proliferative tumor stroma increases the transportation of nanoparticles along the interstitial fiber network and the increased interstitial fluid and slowed lymphatic reflux prolong the retention time of NPs in the tumor stroma. As a result, we detect the accumulation of NPs inside the tumor ISI group. Then the interstitial fluid containing NPs will exchange substances with lymphatic fluid, and the exchanged NPs will return to blood circle at last. So the fluorescence signals are obtained in liver at 24 h in ISI group.

5. Conclusion

To improve antitumor efficacy, we designed PDA-ICG-PTX NPs that exerted synergistic photothermal therapy and chemotherapy effects. *In vitro*, the NPs displayed excellent cytotoxicity. When injected into the interstitial space, these NPs quickly accumulated in the tumor tissue. After irradiation with an 808 nm laser, tumor growth was effectively inhibited due to the synergism of photothermal therapy and chemotherapy with minimal toxicity to other organs. Our study findings indicated that ISI had superior tumor-targeting ability and that the delivered PDA-ICG-PTX NPs have the potential for cancer treatment. This expanded the biological application of NPs.

Ethics approval

All animal experiments adhered to the guideline of the Institutional Animal Care and Use Committee (IACUC) of Chengde Medical University. The IACUC Ethics Committee approved this study with approval number CDMULAC-20210602-009.

Funding

Data availability statement

Data associated with this study has not been deposited into a publicly available repository. Data may be made available on request.

CRediT authorship contribution statement

Yuling Liu: Writing – original draft, Project administration, Methodology, Investigation. **Meng Su:** Writing – original draft, Methodology, Investigation. **Yinghan Wang:** Supervision, Data curation. **Yilong Du:** Validation. **Yan Wang:** Conceptualization. **Nan Hu:** Writing – review & editing, Funding acquisition.

Declaration of competing interest

The authors declare that they have no known competing financial interests or personal relationships that could have appeared to influence the work reported in this paper.

Appendix A. Supplementary data

Supplementary data to this article can be found online at https://doi.org/10.1016/j.heliyon.2024.e27408.

References

[1] B. Chen, W. Dai, B. He, H. Zhang, X. Wang, Y. Wang, Current multistage drug delivery systems based on the tumor microenvironment, Theranostics 7 (3) (2017) 538–558, https://doi.org/10.7150/thno.16684.

[2] D. Cheng, J. Gong, P. Wang, J. Zhu, N. Yu, J. Zhao, 131I-Labeled gold nanoframeworks for radiotherapy-combined second near-infrared photothermal therapy of cancer, J. Mater. Chem. B 9 (45) (2021) 9316–9323, https://doi.org/10.1039/d1tb02115j.

[3] M. Zheng, C. Yue, Y. Ma, P. Gong, P. Zhao, C. Zheng, Z. Sheng, P. Zhang, Z. WangL. Cai, Single-step assembly of DOX/ICG loaded lipid–polymer nanoparticles for highly effective chemo-photothermal combination therapy, ACS Nano 7 (3) (2013) 2056–2067, https://doi.org/10.1021/nn400334y.

[4] M. Izci, C. Maksoudian, B.B. ManshianS, J. Soenen, The use of alternative strategies for enhanced nanoparticle delivery to solid tumors, Chem. Rev. 121 (3) (2021) 1746–1803, https://doi.org/10.1021/acs.chemrev.0c00779.

[5] L. Luo, B. Qin, M. Jiang, L. Xie, Z. Luo, X. Guo, J. Zhang, X. Li, C. Zhu, Y. Du, L. Peng, J. You, Regulating immune memory and reversing tumor thermotolerance through a step-by-step starving-photothermal therapy, NanoBiotechnology 19 (1) (2021) 297, https://doi.org/10.1186/s12951-021-01011-2.

[6] M.R. Morovvati, S.N. Angili, S. Saber-Samandari, M.G. Nejad, D. ToghraieA. Khandan, Global criterion optimization method for improving the porosity of porous scaffolds containing magnetic nanoparticles: fabrication and finite element analysis, Coord. Chem. Rev. (2023), https://doi.org/10.1016/j.ccr.2022.214861.

[7] J. Lu, Y. Yang, Q. Xu, Y. Lin, S. Feng, Y. Mao, D. Wang, S. Wang, Q. Zhao, Recent advances in multi-configurable nanomaterials for improved chemodynamic therapy, Mater. Sci. Eng., B 292 (2023) 116414, https://doi.org/10.1016/j.mseb.2023.116414.

[8] H.T. Nia, L.L. MunnR, K. Jain, Physical traits of cancer, Science 370 (6516) (2020), https://doi.org/10.1126/science.aaz0868 eaaz0868.

[9] N. TracE. J. Chung, Overcoming physiological barriers by nanoparticles for intravenous drug delivery to the lymph nodes, Exp. Biol. Med. 246 (22), 2358-2371, doi:10.1177/15353702211010762..

[10] M.A. Subhan, S.S.K. Yalamarty, N. Filipczak, F. ParveenV, P. Torchilin, Recent advances in tumor targeting via EPR effect for cancer treatment, J. Personalized Med. 11 (6) (2021) 571, https://doi.org/10.3390/jpm11060571.

[11] S. Sindhwani, A.M. Syed, J. Ngai, B.R. Kingston, L. Maiorino, J. Rothschild, P. MacMillan, Y. Zhang, N.U. Rajesh, T. Hoang, J.L.Y. Wu, S. Wilhelm, A. Zilman, S. Gadde, A. Sulaiman, B. Ouyang, Z. Lin, L. Wang, M. EgebladW, C.W. Chan, The entry of nanoparticles into solid tumours, Nat. Mater. 19 (5) (2020) 566–575, https://doi.org/10.1038/s41563-019-0566-2.

[12] I. de LázaroD, J. Mooney, A nanoparticle's pathway into tumours, Nat. Mater. 19 (5) (2020) 486–487, https://doi.org/10.1038/s41563-020-0669-9.

[13] S. Pandit, D. DuttaS. Nie, Active transcytosis and new opportunities for cancer nanomedicine, Nat. Mater. 19 (5) (2020) 478–480, https://doi.org/10.1038/s41563-020-0672-1.

[14] W.T. Liu, Y.P. Cao, X.H. ZhouD, Han, Interstitial fluid behavior and diseases, Adv. Sci. 9 (6) (2022) e2100617, https://doi.org/10.1002/advs.202100617.

[15] P.C. Benias, R.G. Wells, B. Sackey-Aboagye, H. Klavan, J. Reidy, D. Buonocore, M. Miranda, S. Kornacki, M. Wayne, D.L. Carr-LockeN, D. Theise, Structure and distribution of an unrecognized interstitium in human tissues, Sci. Rep. 8 (1) (2018) 4947, https://doi.org/10.1038/s41598-018-23062-6.

[16] O. Cenaj, D.H.R. Allison, R. Imam, B. Zeck, L.M. Drohan, L. Chiriboga, J. Llewellyn, C.Z. Liu, Y.N. Park, R.G. WellsN, D. Theise, Evidence for continuity of interstitial spaces across tissue and organ boundaries in humans, Commun. Biol. 4 (1) (2021) 436, https://doi.org/10.1038/s42003-021-01962-0.

[17] H. Li, Y. Yin, C. Yang, M. Chen, F. Wang, C. Ma, H. Li, Y. Kong, F. JiJ. Hu, Active interfacial dynamic transport of fluid in a network of fibrous connective tissues throughout the whole body, Cell Prolif. 53 (2) (2020) e12760, https://doi.org/10.1111/cpr.12760.

[18] H. Li, C. Yang, Y. Yin, F. Wang, M. Chen, L. Xu, N. Wang, D. Zhang, X. Wang, Y. Kong, Q. Li, S. Su, Y. Cao, W. Liu, Z. Ao, L. Dai, C. Ma, L. Shang, D. Han, F. JiH. Li, An extravascular fluid transport system based on structural framework of fibrous connective tissues in human body, Cell Prolif. 52 (5) (2019) e12667, https://doi.org/10.1111/cpr.12667.

[19] H. Li, B. Li, W. Luo, X. Qi, Y. Hao, C. Yang, W. Li, J. Li, Z. Hua, T. Guo, Z. Zheng, X. Wang, X. Yu, X. Lv, D. Huang, J. Hu, Z. Li, F. Wang, H. Li, C. MaF. Ji, Regulation of adventitial interstitial fluid circulation by heartbeat and respiration, bioRxiv (2022) 2022, https://doi.org/10.1101/2022.10.18.512678, 10.18.512678.

[20] X. Zheng, L. Wang, S. Liu, W. Zhang, F. Liu, Z. Xie, Nanoparticles of chlorin dimer with enhanced absorbance for photoacoustic imaging and phototherapy, Adv. Funct. Mater. 28 (26) (2018), https://doi.org/10.1002/adfm.201706507.

[21] Q. Zhao, Y. Zhang, T. Yu, J. Lu, G. Sun, X. Luo, S. Wang, Tailored nanoplatforms with detachable 'meteorolite' for photothermal-enhanced programmed tumor therapy, Carbon 199 (2022) 119–131, https://doi.org/10.1016/j.carbon.2022.07.073.

[22] Z. Wang, Y. Zou, Y. LiY. Cheng, Metal-containing polydopamine nanomaterials: catalysis, energy, and theranostics, Small 16 (2020).

[23] M. Zhu, Y. Shi, Y. Shan, J. Guo, X. Song, Y. Wu, M. Wu, Y. Lu, W. Chen, X. XuL. Tang, Recent developments in mesoporous polydopamine-derived nanoplatforms for cancer theranostics, J. Nanobiotechnol. 19 (1) (2021) 387, https://doi.org/10.1186/s12951-021-01131-9.

[24] Z. Yuan, C. Lin, Y. He, B. Tao, M. Chen, J. Zhang, P. LiuK. Cai, Near-infrared light-triggered nitric-oxide-enhanced photodynamic therapy and low-temperature photothermal therapy for biofilm elimination, ACS Nano 14 (3) (2020) 3546–3562, https://doi.org/10.1021/acsnano.9b09871.

[25] J. Lu, L. Cai, Y. Dai, Y. Liu, F. Zuo, C. Ni, M. ShiJ. Li, Polydopamine-based nanoparticles for photothermal therapy/chemotherapy and their synergistic therapy with autophagy inhibitor to promote antitumor treatment, Chem. Rec. 21 (4) (2021) 781–796, https://doi.org/10.1002/tcr.202000170.

[26] H. Cheng, Y. He, J. Lu, Z. Yan, L. Song, Y. Mao, D. Di, Y. Gao, Q. Zhao, S. Wang, Degradable iron-rich mesoporous dopamine as a dual-glutathione depletion nanoplatform for photothermal-enhanced ferroptosis and chemodynamic therapy, J. Colloid Interface Sci. 639 (2023) 249–262, https://doi.org/10.1016/j.jcis.2023.02.041.

[27] R. Masuya, M. Matsukubo, K. Nakame, K. Kai, T. Hamada, K. Yano, N. Imamura, M. Hiyoshi, A. NanashimaS. Ieiri, Using indocyanine green fluorescence in laparoscopic surgery to identify and preserve rare branching of the right hepatic artery in pediatric congenital biliary dilatation, Surg. Today 52 (10) (2022) 1510–1513, https://doi.org/10.1007/s00595-022-02516-5.

[28] G. Palomba, V.P. Dinuzzi, G. Sorrentino, M. Capuano, R. Basile, S. Impero, F. Pegoraro, G.D. De PalmaG. Aprea, Iatrogenic biliary leak treated by performing exploratory laparoscopic using indocyanine green (ICG) fluorescence. A case report and review of literature, Ann. Ital. Chir. 11 (2022).

[29] E. Spartalis, G. Ntokos, K. Georgiou, G. Zografos, G. Tsourouflis, D. DimitroulisN, I. Nikiteas, Intraoperative indocyanine green (ICG) angiography for the identification of the parathyroid glands: current evidence and future perspectives, In Vivo 34 (1) (2020) 23–32, https://doi.org/10.21873/invivo.11741.

[30] J. Lin, B. Zheng, S. Lin, Z. ChenS. Chen, The efficacy of intraoperative ICG fluorescence angiography on anastomotic leak after resection for colorectal cancer: a meta-analysis, Int. J. Colorectal Dis. 36 (1) (2021) 27–39, https://doi.org/10.1007/s00384-020-03729-1.

[31] X. Li, T. Yong, Z. Wei, N. Bie, X. Zhang, G. Zhan, J. Li, J. Qin, J. Yu, B. Zhang, L. GanX. Yang, Reversing insufficient photothermal therapy-induced tumor relapse and metastasis by regulating cancer-associated fibroblasts, Nat. Commun. 13 (1) (2022) 2794, https://doi.org/10.1038/s41467-022-30306-7.

[32] D. Jia, D. Liu, S. Zheng, D. Yuan, R. Sun, F. Wang, Y. Li, H. Li, F. Yuan, Q. FanZ. Zhao, ICG-dimeric her2-specific affibody conjugates for tumor imaging and photothermal therapy for her2-positive tumors, Mol. Pharm. 20 (1) (2023) 427–437, https://doi.org/10.1021/acs.molpharmaceut.2c00708.

[33] T.M. Abu Samaan, M. Samec, A. Liskova, P. KubatkaD. Büsselberg, Paclitaxel's mechanistic and clinical effects on breast cancer, Biomolecules 9 (12) (2019), https://doi.org/10.3390/biom9120789.

[34] J. Zhu, J.E. Luo, Y. ChenQ. Wu, Circ_0061140 knockdown inhibits tumorigenesis and improves PTX sensitivity by regulating miR-136/CBX2 axis in ovarian cancer, J. Ovarian Res. 14 (1) (2021) 136, https://doi.org/10.1186/s13048-021-00888-9.

[35] Y.Q. Miao, M.S. Chen, X. Zhou, L.M. Guo, J.J. Zhu, R. Wang, X.X. ZhangY. Gan, Chitosan oligosaccharide modified liposomes enhance lung cancer delivery of paclitaxel, Acta Pharmacol. Sin. 42 (10) (2021) 1714–1722, https://doi.org/10.1038/s41401-020-00594-0.

[36] J. Zhao, Z. Wan, C. Zhou, Q. Yang, J. Dong, X. SongT. Gong, Hyaluronic acid layer-by-layer (LbL) nanoparticles for synergistic chemo-phototherapy, Pharm. Res. (N. Y.) 35 (10) (2018) 196, https://doi.org/10.1007/s11095-018-2480-8.

[37] D. Rahban, M. DoostanA. Salimi, Cancer therapy; prospects for application of nanoparticles for magnetic-based hyperthermia, Cancer Invest. 38 (8–9) (2020) 507–521, https://doi.org/10.1080/07357907.2020.1817482.

[38] N. Hu, Y. Cao, Z. Ao, X. Han, Q. Zhang, W. Liu, S. Liu, F. LiaoD. Han, Flow behavior of liquid metal in the connected fascial space: intervaginal space injection in the rat wrist and mice with tumor, Nano Res.. 11 (4), 2265-2276 doi:10.1007/s12274-017-1848-0..

[39] Y. Li, T. Wen, R. Zhao, X. Liu, T. Ji, H. Wang, X. Shi, J. Shi, J. Wei, Y. Zhao, X. WuG. Nie, Localized electric field of plasmonic nanoplatform enhanced photodynamic tumor therapy, ACS Nano 8 (11) (2014) 11529–11542, https://doi.org/10.1021/nn5047647.

[40] I.A. Khawar, J.H. KimH. J. Kuh, Improving drug delivery to solid tumors: priming the tumor microenvironment, J. Contr. Release 201 (2015) 78–89, https://doi.org/10.1016/j.jconrel.2014.12.018.

[41] B. Chen, W. Dai, B. He, H. Zhang, X. Wang, Y. WangQ. Zhang, Current multistage drug delivery systems based on the tumor microenvironment, Theranostics 7 (3) (2017) 538–558, https://doi.org/10.7150/thno.16684.

[42] M.S. Sudheesh, K. PavithranS. M, Revisiting the outstanding questions in cancer nanomedicine with a future outlook, Nanoscale Adv. 4 (3) (2022) 634–653, https://doi.org/10.1039/d1na00810b.

[43] C. Wong, T. Stylianopoulos, J. Cui, J. Martin, V.P. Chauhan, W. Jiang, Z. Popovic, R.K. Jain, M.G. BawendiD. Fukumura, Multistage nanoparticle delivery system for deep penetration into tumor tissue, Proc. Natl. Acad. Sci. U. S. A. 108 (6) (2011) 2426–2431, https://doi.org/10.1073/pnas.1018382108.

[44] J. Feng, F. Wang, X. Han, Z. Ao, Q. Sun, W. Hua, P. Chen, T. Jing, H. LiD. Han, A "green pathway" different from simple diffusion in soft matter: fast molecular transport within micro/nanoscale multiphase porous systems, Nano Res.. 7 (3), 434-442. doi:10.1007/s12274-014-0409-z..

[45] An in vivo study of the biodistribution of gold nanoparticles after intervaginal space injection in the tarsal tunnel, Nano Res.. 9 (7), 2097-2109. doi:10.1007/s12274-016-1100-3.

[46] N. Hu, X. Shi, Q. Zhang, W. Liu, Y. Zhu, Y. Wang, Y. Hou, Y. Ji, Y. CaoQ. Zeng, Special interstitial route can transport nanoparticles to the brain bypassing the blood-brain barrier, Nano Res.. 12 (11), 2760-2765. doi:10.1007/s12274-019-2510-9..